Dyes and Pigments 205 (2022) 110599

Contents lists available at ScienceDirect

Dyes and Pigments

journal homepage: www.elsevier.com/locate/dyepig

Spectroelectrochemical and ESR investigation of free radicals derived from indotricarbocyanine dyes for photodynamic therapy

Hanna Maltanava [a], Nikita Belko [b,*], Anatol Lugovski [b], Nadzeya Brezhneva [a], Evgeny Bondarenko [c], Pavel Chulkin [c], Grigory Gusakov [b,d], Natalia Vileishikova [d], Michael Samtsov [b,d], Sergey Poznyak [a,**]

[a] Research Institute for Physical Chemical Problems, Belarusian State University, Leningradskaya str. 14, Minsk, 220006, Belarus
[b] A.N. Sevchenko Institute of Applied Physical Problems, Belarusian State University, Kurchatova str. 7, Minsk, 220045, Belarus
[c] Department of Physical Chemistry and Technology of Polymers, Faculty of Chemistry, Silesian University of Technology, Strzody 9, Gliwice, 44-100, Poland
[d] Department of Laser Physics and Spectroscopy, Faculty of Physics, Belarusian State University, Bobruiskaya str. 5, Minsk, 220006, Belarus

ARTICLE INFO

Keywords:
Cyanine dyes
Electrochemistry
UV–Vis spectroscopy
Electron spin resonance
Free radicals
Photodynamic therapy

ABSTRACT

Cyclic voltammetry, UV–Vis absorption spectroscopy, and electron spin resonance are applied to study the properties of indotricarbocyanine dyes and their radicals formed during electrooxidation. We use electrochemistry to generate relatively stable free radicals of the dyes under controlled conditions. The dyes undergo electrooxidation during the chronoamperometric electrolysis at 1.1 V (versus saturated calomel electrode) yielding radical dications. The radicals exhibit an absorption band that is blue-shifted relative to the parent dye (561 nm versus 714 nm). In acetonitrile solutions, the radicals are characterized by a lifetime of *ca.* 20 min and a *g* factor of 2.002. The oxidation potential of the dyes is slightly greater than that of bromide ions allowing the radicals of the dyes to interact with bromide ions. The ability of the indotricarbocyanine dyes to sensitize generation of highly reactive bromine radicals might play an important role in their photodynamic activity.

1. Introduction

Photodynamic therapy (PDT) is a promising and minimally invasive therapeutic method for the treatment of various types of cancer [1–4]. Besides the direct destruction of tumor cells, PDT causes robust antitumor immune responses improving the overall effectiveness of the treatment [5–8]. An essential component of PDT is a photosensitizer (PS), i.e., a chemical compound that intensely accumulates in tumor cells and induces cytotoxicity upon photoactivation. The phototherapeutic window, where biological tissues exhibit maximum transparency, is between 750 and 900 nm [9]. However, many PSs have absorption bands in the 600–700 nm range [2,4,5], which limits the penetration depth of the excitation light into a tumor.

Developing PSs with improved properties remains a very important task. Cyanine dyes have great potential to be used in PDT due to their intense light absorption in the near-infrared (NIR) spectral range, excellent fluorescent characteristics, and low dark toxicity [9–17]. Cyanine dyes provide substantial penetration depth of the excitation light into biological tissues. Another advantage is the tendency of cationic cyanine dyes to accumulate in mitochondria [18] since mitochondria-targeted PDT was found to be particularly effective [11,12].

It is generally accepted that cytotoxicity in PDT is due to the generation of reactive oxygen species [2,4]. As a result, PSs can lose efficiency under hypoxic conditions [16]. Interestingly, cationic indotricarbocyanine dyes with bromide counterion were found to retain photodynamic activity even under hypoxia [19].

In this work, we investigate a cationic indotricarbocyanine dye that has demonstrated high photodynamic activity *in vivo* [20]. PDT with this dye produced an impressive 2.5 cm deep necrotic lesion. The dye was photoactivated at 780 nm, which provided the advantage of the high transparency of biological tissues [21]. Poor water solubility often limits biomedical applications of cyanine dyes [11,16]. Water solubility, biocompatibility, and tumor-to-nontumor specificity of the dye under study were improved by covalent linking of polyethylene glycol substituents to the dye molecules [20].

* Corresponding author.
** Corresponding author.
E-mail addresses: belkoNV@bsu.by (N. Belko), poznyak@bsu.by (S. Poznyak).

https://doi.org/10.1016/j.dyepig.2022.110599
Received 6 June 2022; Received in revised form 15 July 2022; Accepted 17 July 2022
Available online 21 July 2022
0143-7208/© 2022 Elsevier Ltd. All rights reserved.

Although indotricarbocyanine dyes exhibit relatively low singlet oxygen quantum yields (0.01–0.15) [22], they demonstrate high photodynamic activity [19,20,23]. It should be noted that for biomedical applications, the indotricarbocyanine dye is obtained as a bromide salt to improve its solubility in aqueous media. Previously obtained results [24] hint at the ability of the photoexcited molecules of the indotricarbocyanine dye under study to sensitize generation of highly reactive bromine radicals from bromide ions thus inducing cytotoxicity *in vivo*. This assumption could explain retained efficiency of the dye under hypoxia. However, a detailed investigation should be carried out to unveil the origin and role of free radicals in the photodynamic activity of the dye. This information can then be used to improve PDT performance and develop improved PSs.

Generation of common free radicals (e.g., superoxide anion and hydroxyl) in PDT has been addressed in numerous studies [25–29]. To the best of our knowledge, the role of the free radicals of the PS itself is yet to be revealed. Cytotoxicity in PDT is induced by photochemical processes. Such processes can be probed using spectroscopic techniques, such as transient absorption spectroscopy [21,24]. At the same time, studying intermediates of photochemical processes is a challenge as the species can be short-lived (<100 ps lifetime) [21]. Free radicals of cyanine dyes can be produced using electrochemistry [30–32]. Electrochemical methods allow generating relatively stable radicals under controlled conditions and studying their properties (e.g., lifetime, redox characteristics). Electrochemistry also enables us to probe interactions of the generated radicals with other species. Information about the radicals obtained by electrochemical methods can form the basis for a future investigation of photochemical processes involving cyanine dyes.

In this work, we study the formation of radical dications of the cationic indotricarbocyanine dye for PDT and its hydrophobic analogue using electrochemical and spectroelectrochemical methods accompanied by electron spin resonance (ESR) spectroscopy. The redox properties of the dyes as well as the lifetime and *g* factor of their radical dications are determined. The role of the polyethylene glycol substituents on the stability of the radical dications is discussed. The interactions of the radical dications of the dyes with bromide ions are also investigated.

2. Materials and methods

2.1. Synthesis and characterization

The compounds under study are a symmetrical cationic indotricarbocyanine dye **1** (2-[7-[3-dimethyl-1-trimethylene-carboxy-2(1*H*)-indol-2-ylidene]-chloro-3,5-(*o*-phenyleno)-1,2,5-hexatriene-1-yl]-3-dimethyl-1-trimethyl-carboxy-indolium tetrafluoroborate) and its derivative **2** (Fig. 1). Dye **2** was obtained by linking polyethylene glycol with an average molar mass of 300 g·mol^{-1} to dye **1** via ester bonds. Dye **2** is a PS for PDT under development [20]. Hydrophobic dye **1** was studied here for comparison.

Dyes **1** and **2** as their bromide salts were synthesized as described in Ref. 20. The dyes were converted to tetrafluoroborate (BF_4^-) salts for electrochemical studies to exclude reactivity of the counterion. ^{1}H, ^{13}C, and ^{19}F NMR spectra, LC/MS data, and FTIR spectra with band assignment for dyes **1** and **2** as tetrafluoroborate salts can be found in the Supporting Information (Figs. S1–S9, Table S1). The synthetic method for counter-ion exchange and the analytical data for dyes **1** and **2** are presented in the following subsections.

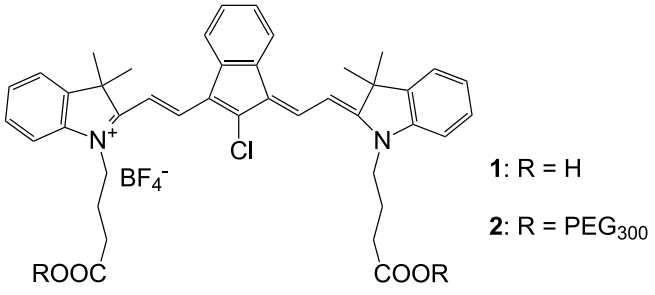

Fig. 1. Molecular structure of dyes **1** and **2**.

2.1.1. Counter-ion exchange method and analytical data for dye *1*

0.5 g (0.67 mmol) of the bromide salt of dye **1** was dissolved in 50 ml of dimethyl sulfoxide. 1.1 g (10 mmol) of sodium tetrafluoroborate in 4 ml of water was added to the dye solution. After 0.5 h, 150 ml of water was added to the mixture. Precipitated dye was filtered from the mixture, washed with water, and air-dried. ^{1}H **NMR** (CD_3CN, 500 MHz) δ 8.32 (s, 2H), 8.12 (s, 2H), 7.65–7.44 (m, 8H), 7.39 (s, 2H), 7.10 (s, 4 H), 4.19 (s, 2H), 3.06–2.04 (m, 8H), 1.77 (s, 12H). **^{13}C NMR** (CD_3CN, 126 MHz) δ 177.95, 175.38, 145.48, 143.02, 142.69, 135.12, 129.89, 127.53, 126.66, 124.73, 123.49, 122.49, 113.15, 103.48, 51.19, 45.35, 41.26, 31.31, 28.31, 23.20, 10.64. **^{19}F NMR** (CD_3CN, 470 MHz) δ −151.80. **MS (ESI)**: *m/z* calculated [M^+] 661.28, found [M^+] 661.4.

2.1.2. Counter-ion exchange method and analytical data for dye *2*

0.3 g (0.25 mmol) of the bromide salt of dye **2** was dissolved in 50 ml of water. 1.1 g (10 mmol) of sodium tetrafluoroborate in 4 ml of water was added to the dye solution. After 0.5 h, the dye was extracted from the aqueous solution with the mixture of 30 ml of dichloroethane and 4 ml of isoamyl alcohol. The organic layer was kept over sodium sulfate. Dichloroethane was removed using a rotary evaporator (the temperature of the fluid bath did not exceed 37 °C), and the dye was precipitated with the mixture of 25 ml of ethyl acetate and 35 ml of diethyl ether. After the mixture was allowed to react for 6 h, the solvent was decanted, and the rest of the reaction mixture was dissolved in 6 ml of methyl ethyl ketone. The solution was filtered, and the dye was precipitated with 50 ml of diethyl ether for 8 h. The solvent was decanted, and the solids were vacuum dried at 22 °C for 3 h. **^{1}H NMR** (CD_3CN, 500 MHz) δ 8.42 (d, J = 15.1 Hz, 2H), 8.16–8.07 (m, 2H), 7.60 (d, J = 7.3 Hz, 2H), 7.53–7.37 (m, 8H), 7.16 (d, J = 15.0 Hz, 2H), 4.34–4.26 (m, 4H), 4.25–4.20 (m, 4H), 3.76–3.34 (m, 46H), 2.65–2.55 (m, 4H), 2.45–2.04 (m, 13H), 1.81 (s, 12H). **^{13}C NMR** (CD_3CN, 126 MHz) δ 178.29, 173.78, 143.47, 143.07, 142.81, 135.19, 129.95, 127.63, 126.44, 124.82, 123.59, 122.38, 113.17, 103.58, 73.31, 73.26, 73.19, 71.02, 69.63, 64.84, 61.97, 61.93, 61.88, 51.33, 45.24, 31.30, 30.81, 28.34, 23.14. **^{19}F NMR** (CD_3CN, 470 MHz) δ −151.78. **MS (ESI)**: $(m/z)_{max}$ calculated 1145.57 [M^+], found 1145.5 [M^+].

2.2. Electrochemistry

Solutions of the dyes under study were prepared in acetonitrile (>99.9%, Merck). Supporting electrolyte for electrochemical measurements was 0.1 M acetonitrile solution of tetra-*n*-butylammonium tetrafluoroborate ($TBABF_4$, >99.0%, Sigma-Aldrich). $TBABF_4$ was vacuum dried for 6 h at 80 °C prior to dissolution in acetonitrile. Tetra-*n*-butylammonium bromide (TBABr, >99.0%, Sigma-Aldrich) was used as a source of bromide ions.

Cyclic voltammetry experiments were carried out in an airtight, three-electrode cell that was made of pyrex and included a working electrode, a counter-electrode, and a reference electrode. A Pt disc (0.4 mm diameter) was used as the working electrode. The counter electrode was a coiled Pt wire. The Ag/Ag^+ reference electrode was made of a coiled Ag wire submerged in a 0.01 M acetonitrile solution of $AgBF_4$. The potential of the reference electrode was measured against Fc^+/Fc couple and found to be 0.32 V vs. saturated calomel electrode (SCE). All potentials in this work were recalculated vs. SCE. Cyclic voltammetry was performed at room temperature (20±2 °C) using an Autolab PGSTAT 302N potentiostat. The solutions were deaerated prior to the measurements by repeated (20–25 times) cycles of evacuation and subsequent purging with argon. During the measurements, the electrochemical cell

was hermetically sealed and kept under an overpressure of argon.

Chronoamperometric electrolysis was carried out in the same electrochemical cell. In this case, the working electrode was a Pt plate (11 × 43 mm, 9.5 cm^2 area). The working electrode compartment was separated from the counter-electrode compartment by a membrane permeable for the supporting electrolyte but impermeable for the molecules of dyes **1** and **2**. During electrolysis, a solution was circulated through a 1 mm quartz cell (Hellma, 170-000-1-40) using a peristaltic pump, and its UV–Vis absorption spectrum was periodically measured on a monochromator-based Solar PV1251 spectrophotometer. The data acquisition in the 315–900 nm range was performed by scanning the wavelength and required 2 min. In our experiments, the absorbance changed with the rate not exceeding 4×10^{-2} min^{-1}. As a result, the deformation of the spectra during the scanning of the wavelength was negligible. Hermetic conditions were maintained in the electrochemical cell and in the quartz cell throughout the measurements.

2.3. ESR spectroscopy

ESR measurements were performed using a JEOL JES FA-200 spectrometer. The custom-made glass cell for combined electrochemistry–ESR experiments contained 2 mL of a solution and included three electrodes. The working electrode and the counter-electrode were Pt wires. The reference electrode was an Ag wire submerged in a 0.01 M acetonitrile solution of $AgNO_3$ (Ag/Ag^+ reference electrode). The reference electrode compartment was separated from the rest of the cell by a salt bridge filled with a 0.1 M acetonitrile solution of $TBABF_4$. The potential of the electrodes was controlled with an Autolab PGSTAT 302N potentiostat. The potential of the reference electrode was calibrated against Fc^+/Fc couple and found to be 0.32 V vs. SCE. The solutions were purged with nitrogen for 40 min before the measurements. ESR spectra were recorded in two sweeps with a total accumulation time of 30 s. The field modulation and the amplitude were set to 1 mT and 200 mT, respectively, and the center of the field was positioned at 340.5 mT. The *g* factors of the dyes under study were calculated with respect to the fourth line of a Mn reference with a known *g* factor of 1.981.

3. Results and discussion

3.1. Cyclic voltammetry and ESR spectroscopy

Redox processes involving the molecules of dyes **1** and **2** were studied using cyclic voltammetry. The potential was swept in the anodic direction relative to the equilibrium potential of the working electrode. The cyclic voltammograms for both dyes exhibit an intense oxidation wave at *ca.* 0.90 V (Fig. 2). The subsequent reduction wave is more pronounced for dye **2**. We can assume that the bulky polyethylene glycol substituents of dye **2** have little effect on the position of the oxidation wave but possibly lead to retarded diffusion of dye molecules. For the scan rates between 5 and 200 $mV{\cdot}s^{-1}$, the amplitude of the oxidation wave scales linearly with the square root of the scan rate (Fig. S10). This dependence indicates that electrooxidation is electrochemically reversible [33] and the rate of this process is limited by the diffusion of the dye molecules to the electrode surface [34]. At scan rates below 50 $mV{\cdot}s^{-1}$, the reduction wave is virtually absent in the cyclic voltammograms (Fig. S10a). This effect at low scan rates could be due to diffusion of the electrogenerated species away from the electrode. Additional information on the voltammetric behavior of dyes **1** and **2** can be found in our previous work [35].

Electrooxidation of the dyes under study leads to the formation of their radical dications (Fig. 3). A similar process was observed for cationic cyanine dyes with different molecular structures [30,31].

Formation of the radical dications of dyes **1** and **2** was confirmed by ESR spectroscopy (Fig. 4). The radicals were generated by electrooxidation at 1.1 V. The ESR spectra for the dyes measured during electrolysis are broad and featureless. The radicals of both dyes are

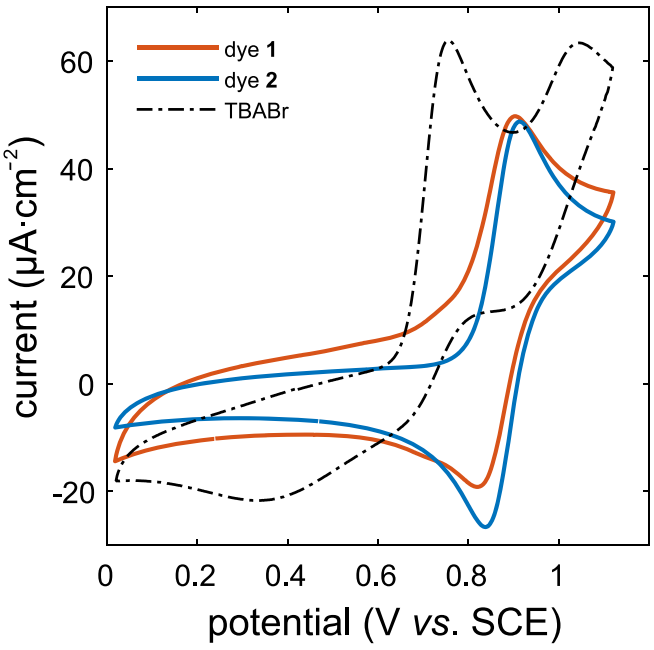

Fig. 2. Cyclic voltammograms for 0.1 mM solutions of dye **1** (red curve), dye **2** (blue curve), and TBABr (dash-dotted black curve) in the supporting electrolyte recorded at a scan rate of 200 $mV{\cdot}s^{-1}$.

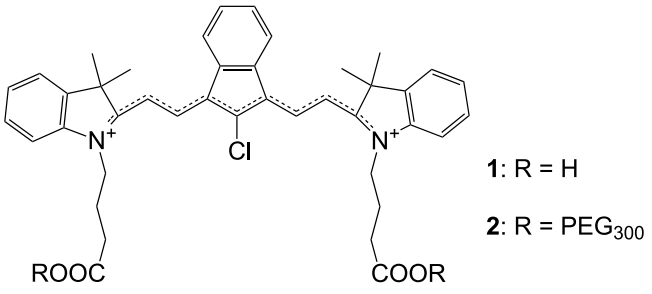

Fig. 3. Radical dications of dyes **1** and **2**.

characterized by the same *g* factor of 2.002 indicative of a high extent of electron delocalization. The measured *g* value is typical of free radicals of organic species. Similar ESR signals were observed for various cyanine dye/AgBr [36–40] or cyanine dye/titanate [41] systems as the result of light-induced oxidation of dye molecules.

Fig. 5 shows the intensity of the ESR signals during anodic polarization as a function of the electrode potential. The ESR spectra were recorded after 1 min of polarization in potentiostatic regime with a potential step of 0.05 V. The intensity of the ESR signals is proportional to the transient radical concentration resulting from the formation and decay of the radical dications of the dyes during electrooxidation. The ESR signals of the radical dications appear at 0.75–0.8 V for both dyes and level off at 1.1 V. The decrease in the ESR signals for potentials greater than 1.1 V can be related to side reactions.

3.2. UV–Vis absorption spectroscopy and chronoamperometric electrolysis

The UV–Vis absorption spectra for dyes **1** and **2** in acetonitrile exhibit an intense band peaked at 714 nm with a shape typical of cyanine dyes [42,43] (Fig. 6). The short-wavelength shoulder of the band can be assigned to the electronic transition coupled to the symmetric vinyl stretching vibrational mode [43–45]. Additional weak

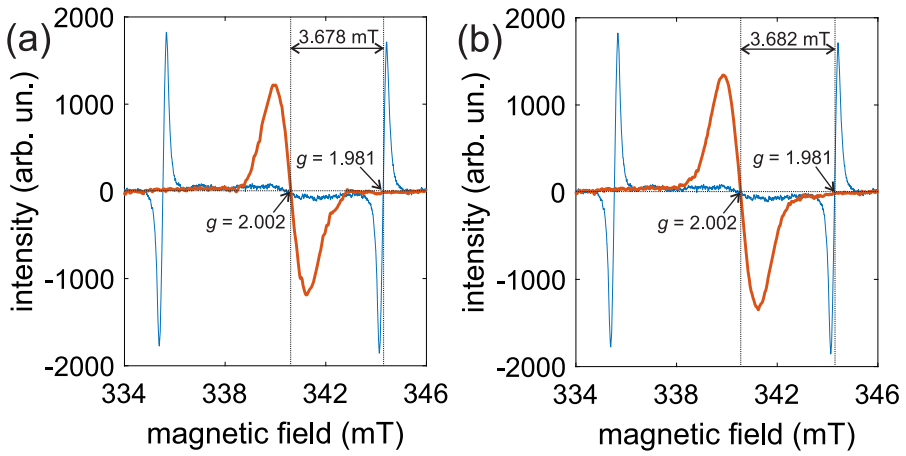

Fig. 4. The red curves depict ESR spectra for 0.1 mM solutions of dye **1** (a) and dye **2** (b) in the supporting electrolyte measured during electrolysis at 1.1 V. The blue curves show the spectrum for a Mn reference.

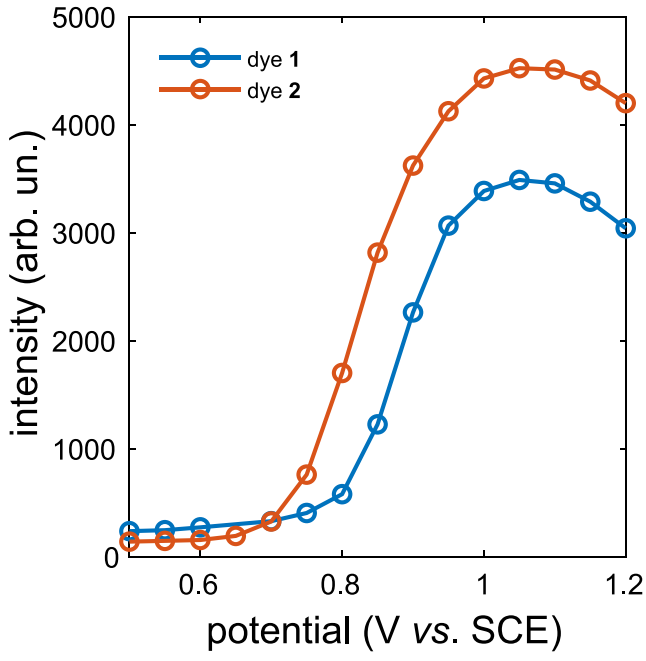

Fig. 5. Dependence of the intensity of the ESR signal on the applied potential for dye **1** (blue curve) and dye **2** (red curve) in the supporting electrolyte.

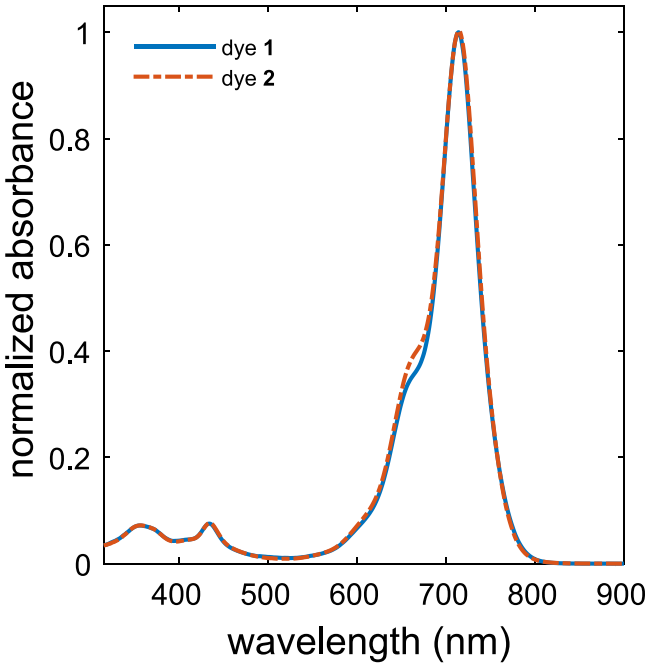

Fig. 6. Normalized UV–Vis absorption spectra for 0.1 mM solutions of dye **1** (blue curve) and dye **2** (dash-dotted red curve) in the supporting electrolyte.

absorption bands at 355 and 434 nm correspond to transitions to high-lying electronic states [46–48]. Absorption spectra for dyes **1** and **2** are virtually identical indicating negligible influence of the polyethylene glycol substituents on the chromophore, i.e., the polymethine chain. In polar solvents, cationic cyanine dyes exist only in the monomeric form and are completely dissociated [42,49]. As a result, monomeric cations of **1** or **2** are the only type of absorbers in polar acetonitrile. Addition of 0.1 M $TBABF_4$ has no influence on the absorption spectra of the dye solutions and thus does not inhibit the dissociation of the dyes.

Solutions of dyes **1** and **2** were subjected to chronoamperometric electrolysis at 1.1 V (vs. SCE). According to the cyclic voltammetry data (Fig. 2), this potential is sufficient to induce the electrooxidation of the dyes. The transformations of the dyes during electrolysis were monitored using UV–Vis absorption spectroscopy. Dyes **1** and **2** exhibited similar behavior, and here we present the data for dye **2**; the data for dye **1** can be found in the Supporting Information.

Under applied potential, a new absorption band appears at 561 nm (Fig. 7a and S11a). This band can be attributed to the generated radical dication of the parent dye. Absorbance at 561 nm reaches its maximum value after 45 min (31 min) of electrolysis for dye **2** (dye **1**) and then starts to decay (Fig. 7b and S11b). Absorbance at 714 nm is steadily decreasing. The observed evolution of the absorption spectra indicates that the electrooxidation of the parent dye yields additional products besides the radical dication.

After stopping the anodic polarization, the absorption band of the radical dication gradually disappears, and the band of the parent dye is partially recovered (Fig. 8a and S12a). Decay of the absorbance at 561 nm is well fitted with a single exponential function (Fig. 8b and S12b). As follows from Fig. 8b, the lifetime of the radical dications of dye **2** in a deaerated acetonitrile solution is 26 min. The radical dications of dye **1** are characterized by a shorter lifetime of 16 min (Fig. S12b). Dye **2** also exhibits the more intense ESR signal compared to dye **1** (Fig. 5), hinting at higher radical persistence. The higher persistence of the radicals for dye **2** could be due to protection of the chromophore by the bulky polyethylene glycol substituents.

As shown previously [50], the radical dications of cyanine dyes with a free polymethine chain have a tendency to dimerize rapidly, forming a covalent bond between even methine carbon atoms. On the contrary, alkyl substitution at the methine carbons electronically stabilizes the radicals and sterically inhibits their dimerization [30]. The chloro-*o*-phenyleno substituent incorporated within the polymethine chain of dyes **1** and **2** probably inhibits dimerization of their radical dications.

The absorption band of the radical dications completely disappears 75 min after the anodic polarization is stopped. At this point, the band of the parent dye recovers to 46% of its initial value measured before electrolysis (Fig. 9). The rest of the parent dye is transformed irreversibly yielding products responsible for the increased absorption in the 315–500 nm range. The products of the irreversible processes can be compounds with disrupted conjugation in the polymethine chain, since their absorption is blue-shifted relative to the parent dye.

To gain insight in the nature of the irreversible processes, we calculated the total charge $q_{total}(t)$ that is transported through the dye solution during electrolysis using Eq. (1):

$$q_{total}(t) = \int_0^t I_{anodic}(\tau)d\tau, \quad (1)$$

where $I_{anodic}(t)$ is the anodic current measured at the working electrode during electrolysis.

The absorption bands of the parent dye and its radical dication practically do not overlap. Consequently, the absorbance at 714 nm is directly proportional to the amount of the parent dye present in the solution. The amount of the electrooxidized dye can thus be calculated using Eq. (2):

$$m_{ox} = m_{total}\frac{|A(t) - A_0|}{A_0}, \quad (2)$$

where m_{total} is the total mass of the parent dye present in the solution; A_0 is the absorbance at 714 nm before electrolysis; $A(t)$ is the absorbance at 714 nm at various times during electrolysis.

We assume that the electrooxidation of the parent dye is a one-electron process. The charge $q_{dye}(t)$ resulting from the electrooxidation of the parent dye can thus be calculated using Eq. (3):

$$q_{dye}(t) = \frac{FZm_{ox}(t)}{M}, \quad (3)$$

where $F = 96485$ C·mol^{-1} is the Faraday constant; $Z = 1$ is the number of electrons transferred from each dye molecule; $m_{ox}(t)$ is the mass of the parent dye that was oxidized during electrolysis; M is the molar mass of the dye.

During electrolysis, $q_{dye}(t)$ follows a time trace with an inflection point (Fig. 10 and S13) and displays a slower rate of growth during the first 5 min. On the contrary, $q_{total}(t)$ follows a time trace that is concave downward in the whole range. The ratio $q_{dye}(t)/q_{total}(t)$ (Fig. 10, dash-dotted purple curve) and the absorbance of the radical dications (Fig. 7b, red curve) simultaneously reach their maximum value after ~40 min of electrolysis. The solution probably contains trace amounts of impurities that are preferentially electrooxidized at the initial stage of electrolysis retarding the generation of the radicals. After that, a dynamic equilibrium is established between the generation of the radicals at the working electrode and the decay of the radicals. After the depletion of the parent dye, the equilibrium shifts towards the decay of the radical dications. The peak value for the ratio $q_{dye}(t)/q_{total}(t)$ is only 30%. This might indicate that the electrooxidation of the same dye molecule and the reduction of its radical dication can occur several times during electrolysis.

3.3. The effect of bromide ions

As mentioned in the Introduction, indotricarbocyanine dyes might sensitize generation of bromine radicals from bromide ions. At first, we studied redox properties of pure bromide ions using cyclic voltammetry. The cyclic voltammogram for a 0.1 mM solution of TBABr in the supporting electrolyte exhibits two anodic waves at 0.76 and 1.05 V (Fig. 2, dash-dotted black curve). According to previously reported data, the first wave can be assigned to the electrooxidation of bromide ions to elementary bromine (Eq. (4)) followed by formation of tribromide ions (Eq. (5)) [51,52]:

$$2Br^- - 2e^- \longrightarrow Br_2 \quad (4)$$

$$Br_2 + Br^- \longleftrightarrow Br_3^- \quad (5)$$

Tribromide ions are sufficiently stable in acetonitrile and are further electrooxidized (Eq. (6)), resulting in the appearance of the second wave in the voltammogram:

$$2Br_3^- - 2e^- \longrightarrow 3Br_2 \quad (6)$$

As follows from the cyclic voltammetry data (Fig. 2), the oxidation potential for dyes **1** and **2** is slightly greater than the oxidation potential for bromide ions. To study the interactions of bromide ions with the products of the dye electrooxidation, solutions of **1** or **2** with an equimolar amount of TBABr were subjected to chronoamperometric electrolysis at 1.1 V. During the first 30 min of electrolysis, the absorption

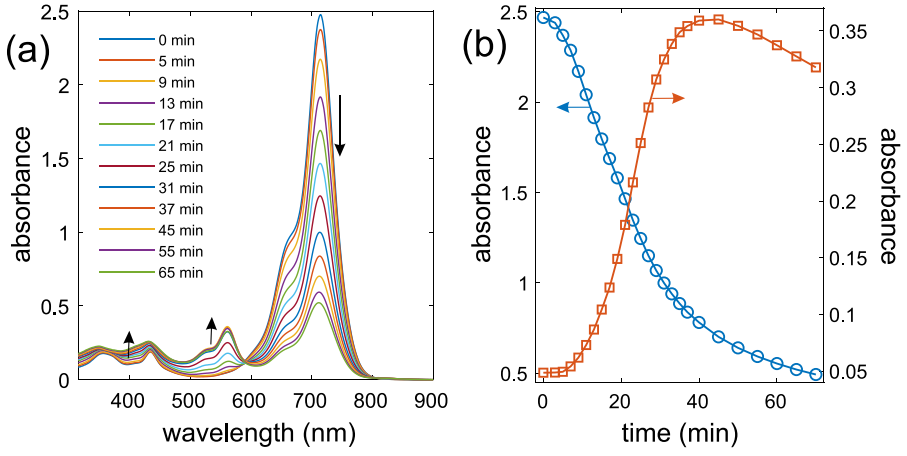

Fig. 7. (a) Evolution of the absorption spectrum for a 0.1 mM solution of dye **2** in the supporting electrolyte during electrolysis at 1.1 V for 65 min. The spectra were recorded at the times indicated in the legend after starting electrolysis. (b) Absorbance of the parent dye at 714 nm (blue curve) and of the radical dication at 561 nm (red curve) vs. time during electrolysis.

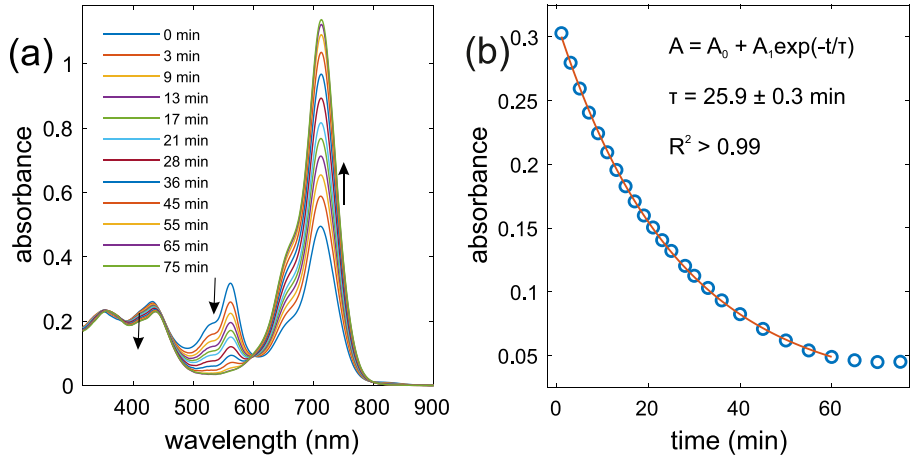

Fig. 8. (a) Evolution of the absorption spectrum for a 0.1 mM solution of dye **2** in the supporting electrolyte for 75 min after stopping electrolysis at 1.1 V. The spectra were recorded at the times indicated in the legend after stopping electrolysis. (b) Absorbance of the radical dication at 561 nm vs. time elapsed after stopping electrolysis (blue symbols) and the fitting exponential function (red curve). The parameters of the fitting function are shown in the legend.

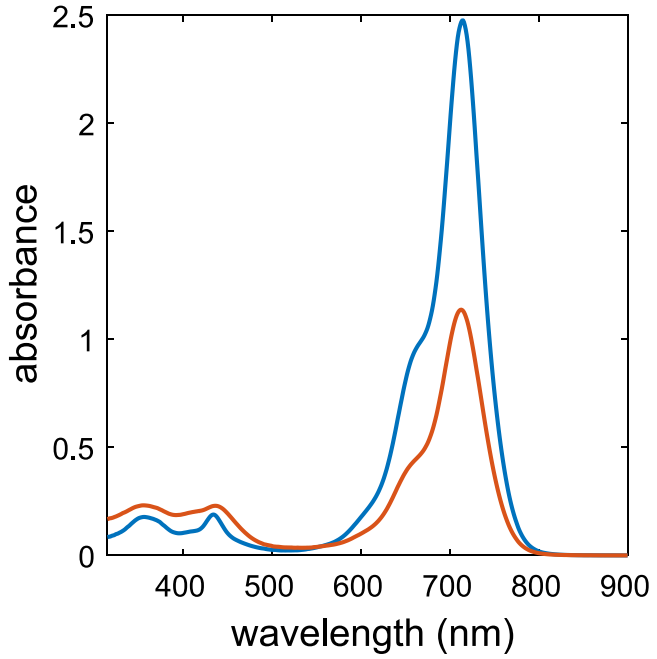

Fig. 9. Absorption spectra for a 0.1 mM solution of dye **2** in the supporting electrolyte before electrolysis at 1.1 V (blue curve) and at 75 min after (red curve) stopping electrolysis.

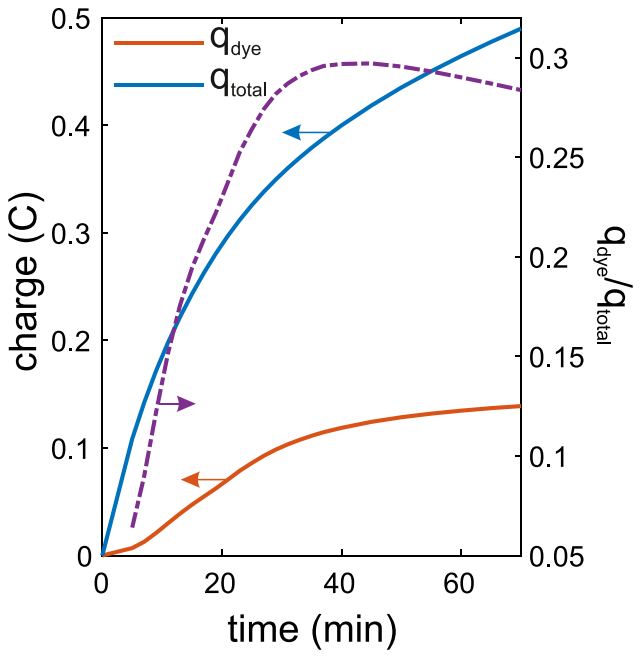

Fig. 10. Total charge transported through a 0.1 mM solution of dye **2** ($q_{total}(t)$, blue curve) during electrolysis, the charge resulting from the electrooxidation of dye **2** ($q_{dye}(t)$, red curve), and the ratio $q_{dye}(t)/q_{total}(t)$ (dash-dotted purple curve) vs. time.

band at 714 nm is decaying, while the absorbance at 561 nm is changing insignificantly. After 30 min of electrolysis, the band at 561 nm appears and increases over time (Fig. S14a). Thus, we can assume that bromide ions are preferentially electrooxidized during the first 30 min of electrolysis. As the concentration of bromide ions drops, generation of the radical dications of **1** or **2** becomes more probable. The peak value for the ratio $q_{dye}(t)/q_{total}(t)$ is only 20% (Fig. S14b), which is even less than the value observed in the absence of bromide ions (Fig. 10). This confirms that the anodic current in part results from the electrooxidation of bromide ions.

The presence of TBABr also significantly decreases the ESR signal for the solutions of the dyes during electrolysis (Fig. S15). This finding confirms the ability of bromide ions to inhibit the generation of the radical dications of the dyes.

It is also important to investigate the interactions between bromide ions and the radical dications of the dyes. For that purpose, the radical dications are generated first by subjecting a solution of dye **2** to electrolysis at 1.1 V for 55 min. An equimolar amount of bromide ions is then injected into the electrochemical cell. The color of the solution changes immediately from crimson to deep green. After 1 min, the band at 561 nm is absent in the absorption spectrum, and the band at 714 nm is partially recovered (Fig. 11). There is thus evidence that the radical dications of **1** or **2** can oxidize bromide ions, which results in a partial recovery of the parent dye.

4. Conclusions

Electrooxidation of the indotricarbocyanine dyes in acetonitrile was shown to yield radical dications with a lifetime of *ca.* 20 min and a *g*

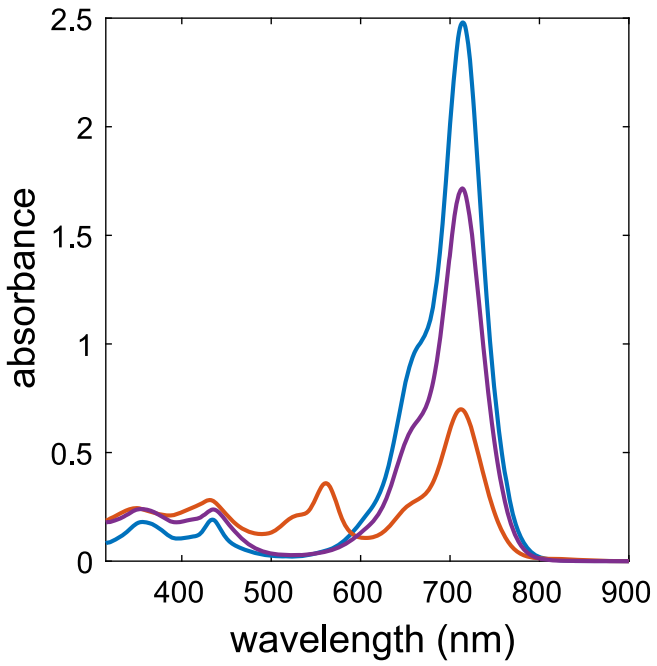

Fig. 11. Absorption spectra for a 0.1 mM solution of dye **2** in the supporting electrolyte before electrolysis (blue curve), after 55 min of electrolysis at 1.1 V (red curve), and at 1 min after subsequent addition of an equimolar amount of TBABr (purple curve).

factor of 2.002. Persistence of the radicals and reversibility of their formation is probably due to the chloro-*o*-phenyleno substituent incorporated within the polymethine chain. The polyethylene glycol substituents in the dye molecules further increase the stability of the radical dications. The dye electrooxidation is also followed by irreversible processes yielding products with disrupted conjugation in the polymethine chain.

When the parent dye and bromide ions are present in the solution simultaneously, bromide ions are preferentially oxidized before the formation of the radical dications of the dye begins. When bromide ions are injected into the solution already containing the radical dications of the dye, bromide ions are rapidly oxidized and the parent dye is partially recovered. The formation of highly reactive bromine radicals might be observed in the course of such transformations.

These findings will be applied to study photochemical processes involving the molecules of cyanine dyes. Future work will also entail studying indotricarbocyanine dyes with other substituents.

Author contribution statement

Hanna Maltanava: Data Curation, Investigation, Methodology, Writing – original manuscript. **Nikita Belko:** Data Curation, Investigation, Visualization,Writing – original manuscript. **Anatol Lugovski:** Conceptualization, Resources, Synthesis. **Nadzeya Brezhneva:** Data Curation, Investigation. **Evgeny Bondarenko:** Data Curation, Investigation, Visualization. **Pavel Chulkin:** Conceptualization, Supervision. **Grigory Gusakov:** Sample Preparation, Investigation, Data Curation. **Natalia Vileishikova:** Investigation, Data Curation. **Michael Samtsov:** Conceptualization, Supervision, Resources, Writing – review editing. **Sergey Poznyak:** Conceptualization, Investigation, Supervision, Writing – review editing.

Declaration of competing interest

The authors declare the following financial interests/personal relationships which may be considered as potential competing interests:

Hanna Maltanava reports financial support was provided by Belarusian Republican Foundation for Fundamental Research. Hanna Maltanava reports financial support was provided by Polish National Agency for Academic Exchange. Nikita Belko reports financial support was provided by Belarusian Republican Foundation for Fundamental Research. Nikita Belko reports financial support was provided by State Program of Scientific Research of the Republic of Belarus. Anatol Lugovski reports financial support was provided by State Program of Scientific Research of the Republic of Belarus. Nadzeya Brezhneva reports financial support was provided by Polish National Agency for Academic Exchange. Michael Samtsov reports financial support was provided by Belarusian Republican Foundation for Fundamental Research. Michael Samtsov reports financial support was provided by State Program of Scientific Research of the Republic of Belarus.

Data availability

Data will be made available on request.

Acknowledgements

This work was supported by the Belarusian Republican Foundation for Fundamental Research (project numbers F22MB-014 and F22UZB-044); the Polish National Agency for Academic Exchange within the scope of PROM2020 program; the state program of scientific research of the Republic of Belarus “Photonics and Electronics for Innovation” (grant number 20211268); and the state program of scientific research of the Republic of Belarus “Convergence” (grant number 20211236).

Appendix A. Supplementary data

Supplementary data to this article can be found online at https://doi.org/10.1016/j.dyepig.2022.110599.

References

[1] Celli JP, Spring BQ, Rizvi I, Evans CL, Samkoe KS, Verma S, Pogue BW, Hasan T. Imaging and photodynamic therapy: mechanisms, monitoring, and optimization. Chem Rev 2010;110:2795–838.
[2] Agostinis P, Berg K, Cengel KA, Foster TH, Girotti AW, Gollnick SO, Hahn SM, Hamblin MR, Juzeniene A, Kessel De a. Photodynamic therapy of cancer: an update. CA A Cancer J Clin 2011;61:250–81.
[3] Tampa M, Sarbu M-I, Matei C, Mitran C-I, Mitran M-I, Caruntu C, Constantin C, Neagu M, Georgescu S-R. Photodynamic therapy: a hot topic in dermato-oncology. Oncol Lett 2019;17:4085–93.
[4] Gunaydin G, Gedik ME, Ayan S. Photodynamic therapy for the treatment and diagnosis of cancer–a review of the current clinical status. Front Chem 2021;9:608.
[5] Donohoe C, Senge MO, Arnaut LG, Gomes-da Silva LC. Cell death in photodynamic therapy: from oxidative stress to anti-tumor immunity. Biochim Biophys Acta, Rev Cancer 2019;1872:188308.
[6] Sun X, Cao Z, Mao K, Wu C, Chen H, Wang J, Wang X, Cong X, Li Y, Meng X, et al. Photodynamic therapy produces enhanced efficacy of antitumor immunotherapy by simultaneously inducing intratumoral release of sorafenib. Biomaterials 2020; 240:119845.
[7] He C, Duan X, Guo N, Chan C, Poon C, Weichselbaum RR, Lin W. Core-shell nanoscale coordination polymers combine chemotherapy and photodynamic therapy to potentiate checkpoint blockade cancer immunotherapy. Nat Commun 2016;7:1–12.
[8] Zheng Y, Yin G, Le V, Zhang A, Chen S, Liang X, Liu J. Photodynamic-therapy activates immune response by disrupting immunity homeostasis of tumor cells, which generates vaccine for cancer therapy. Int J Biol Sci 2016;12:120.
[9] Atchison J, Kamila S, Nesbitt H, Logan KA, Nicholas DM, Fowley C, et al. Iodinated cyanine dyes: a new class of sensitisers for use in NIR activated photodynamic therapy (PDT). Chem Commun 2017;53:2009–12.
[10] Shi C, Wu JB, Pan D. Review on near-infrared heptamethine cyanine dyes as theranostic agents for tumor imaging, targeting, and photodynamic therapy. J Biomed Opt 2016;21:50901.
[11] Thomas AP, Palanikumar L, Jeena M, Kim K, Ryu J-H. Cancer-mitochondria-targeted photodynamic therapy with supramolecular assembly of HA and a water soluble NIR cyanine dye. Chem Sci 2017;8:8351–6.
[12] Usama SM, Thavornpradit S, Burgess K. Optimized heptamethine cyanines for photodynamic therapy. ACS Appl Bio Mater 2018;1:1195–205.
[13] James NS, Cheruku RR, Missert JR, Sunar U, Pandey RK. Measurement of cyanine dye photobleaching in photosensitizer cyanine dye conjugates could help in

optimizing light dosimetry for improved photodynamic therapy of cancer. Molecules 2018;23:1842.
[14] Zhao X, Yang Y, Yu Y, Guo S, Wang W, Zhu S. A cyanine-derivative photosensitizer with enhanced photostability for mitochondria-targeted photodynamic therapy. Chem Commun 2019;55:13542–5.
[15] Yang X, Bai J, Qian Y. The investigation of unique water-soluble heptamethine cyanine dye for use as NIR photosensitizer in photodynamic therapy of cancer cells. Spectrochim Acta A Mol Biomol Spectrosc 2020;228:117702.
[16] Lange N, Szlasa W, Saczko J, Chwiłkowska A. Potential of cyanine derived dyes in photodynamic therapy. Pharmaceutics 2021;13:818.
[17] Bilici K, Cetin S, Aydındogan E, Yagci Acar H, Kolemen S. Recent advances in cyanine-based phototherapy agents. Front Chem 2021:444.
[18] Delaey E, van Laar F, De Vos D, Kamuhabwa A, Jacobs P, de Witte P. A comparative study of the photosensitizing characteristics of some cyanine dyes. J Photochem Photobiol B Biol 2000;55:27–36.
[19] Istomin YP, Alexandrova E, Zhavrid E, Voropay E, Samtsov M, Kaplevsky K, et al. The effect of hypoxia on photocytotoxicity of TICS tricarbocyanine dye in vitro. Exp Oncol 2006;28:1–3.
[20] Lugovski A, Samtsov MP, Kaplevsky KN, Tarasau D, Voropay ES, Petrov PT, et al. Novel indotricarbocyanine dyes covalently bonded to polyethylene glycol for theranostics. J Photochem Photobiol A Chem 2016;316:31–6.
[21] Samtsov M, Tikhomirov S, Buganov O, Kaplevsky KN, Melnikov D, Lyashenko L. Fast photoprocesses in a symmetric indotricarbocyanine dye (HITC) in solutions. J Appl Spectrosc 2009;76:783–90.
[22] Samtsov M, Voropai E, Kaplevskii K, Mel'nikov D. Generation of singlet oxygen by indotricarbocyanine dyes in low-polarity media. J Appl Spectrosc 2008;75:692–9.
[23] Samtsov M, Voropay E, Kaplevsky K, Melnikau D, Lyashenko L, Istomin YP. Influence of photon energy on the efficiency of photochemotherapy. J Appl Spectrosc 2009;76:547–53.
[24] Samtsov M, Tikhomirov S, Lyashenka L, Tarasau D, Buganov O, Galievsky V, et al. Photophysical and photochemical properties of HITC indotricarbocyanine dye molecules in solutions. J Appl Spectrosc 2013;80:170–5.
[25] Price M, Reiners JJ, Santiago AM, Kessel D. Monitoring singlet oxygen and hydroxyl radical formation with fluorescent probes during photodynamic therapy. Photochem Photobiol 2009;85:1177–81.
[26] Li M, Xia J, Tian R, Wang J, Fan J, Du J, Long S, Song X, Foley JW, Peng X. Near-infrared light-initiated molecular superoxide radical generator: rejuvenating photodynamic therapy against hypoxic tumors. J Am Chem Soc 2018;140:14851–9.
[27] Zhang K, Yu Z, Meng X, Zhao W, Shi Z, Yang Z, Dong H, Zhang X. A bacteriochlorin-based metal–organic framework nanosheet superoxide radical generator for photoacoustic imaging-guided highly efficient photodynamic therapy. Adv Sci 2019;6:1900530.
[28] Wan Q, Zhang R, Zhuang Z, Li Y, Huang Y, Wang Z, et al. Molecular engineering to boost AIE-active free radical photogenerators and enable high-performance photodynamic therapy under hypoxia. Adv Funct Mater 2020;30:2002057.
[29] Cui X, Lu G, Dong S, Li S, Xiao Y, Zhang J, Liu Y, Meng X, Li F, Lee C-S. Stable π-radical nanoparticles as versatile photosensitizers for effective hypoxia-overcoming photodynamic therapy. Mater Horiz 2021;8:571–6.
[30] Lenhard J, Parton R. Electrochemical and spectroscopic analyses of the thermodynamics of the reversible dimerization of cyanine radical dications. J Am Chem Soc 1987;109:5808–13.
[31] Lenhard J, Cameron A. Electrochemistry and electronic spectra of cyanine dye radicals in acetonitrile. J Phys Chem 1993;97:4916–25.
[32] Lee SK, Richter MM, Strekowski L, Bard AJ. Electrogenerated chemiluminescence. 61. near-IR electrogenerated chemiluminescence, electrochemistry, and spectroscopic properties of a heptamethine cyanine dye in MeCN. Anal Chem 1997;69:4126–33.
[33] Bard AJ, Faulkner LR. Electrochemical methods: fundamentals and applications. John Wiley & Sons; 2001.
[34] Evans DH, O'Connell KM, Petersen RA, Kelly MJ. Cyclic voltammetry. J Chem Educ 1983;60:290.
[35] Maltanava H, Poznyak S, Belko N, Samtsov M. Optical and electrochemical properties of indotricarbocyanine dyes for photodynamic therapy. J Appl Spectrosc 2021;88:489–95.
[36] Needler W, Griffith R, West W. Electron spin resonance absorptions induced by light in adsorbed layers of cyanine dyes on silver bromide microcrystals. Nature 1961;191:902–3.
[37] Tani T, Sano Y. Factors influencing light-induced ESR spectra of dyes adsorbed by AgBr emulsion grains. J Photogr Sci 1979;27:231–40.
[38] Tani T. Electron-spin resonance and photographic effect of positive holes trapped by cyanine dyes adsorbed on silver bromide microcrystals. J Appl Phys 1987;62:2456–60.
[39] Ceulemans T, Schoemaker D, Vandenbroucke D, De Keyzer R. Formation and decay kinetics of light-induced dye radicals on spectrally sensitized AgBr microcrystals measured by electron spin resonance spectroscopy: a quantitative model. J Appl Phys 1997;82:1776–83.
[40] Van Nylen J, Schoemaker D, Goovaerts E, Callant P, Viaene K, De Keyzer R. Elucidation by electron spin resonance and optical spectroscopy of the supersensitization mechanism in a red-sensitive AgCl-based photographic emulsion. J Appl Phys 2004;96:3187–92.
[41] Miyamoto N, Kuroda K, Ogawa M. Visible light induced electron transfer and long-lived charge separated state in cyanine dye/layered titanate intercalation compounds. J Phys Chem B 2004;108:4268–74.
[42] Ishchenko AA. Structure and spectral-luminescent properties of polymethine dyes. Russ Chem Rev 1991;60:865.
[43] Mustroph H, Reiner K, Mistol J, Ernst S, Keil D, Hennig L. Relationship between the molecular structure of cyanine dyes and the vibrational fine structure of their electronic absorption spectra. ChemPhysChem 2009;10:835–40.
[44] Spano FC. The spectral signatures of frenkel polarons in H- and J-aggregates. Acc Chem Res 2010;43:429–39.
[45] Mustroph H. Cyanine dyes. Phys Sci Rev 2020;5.
[46] Svetlichnyi V, Samtsov M, Bazyl O, Smirnov O, Mel'nikov D, Lugovskii A. Optical properties of new indotricarbocyanine dye as a limiter of laser radiation power. J Appl Spectrosc 2007;74:524–32.
[47] Kasatani K, Sato H. Viscosity-dependent decay dynamics of the S2 state of cyanine dyes with 3, 5, and 7 methine units by picosecond fluorescence lifetime measurements. Bull Chem Soc Jpn 1996;69:3455–60.
[48] Guarin CA, Villabona-Monsalve JP, López-Arteaga R, Peon J. Dynamics of the higher lying excited states of cyanine dyes. an ultrafast fluorescence study. J Phys Chem B 2013;117:7352–62.
[49] Chibisov AK, Zakharova GV, Görner H. Photoprocesses in dimers of thiacarbocyanines. Phys Chem Chem Phys 1999;1:1455–60.
[50] Parton R, Lenhard J. Dimerization reactions of cyanine radical dications. J Org Chem 1990;55:49–57.
[51] Allen GD, Buzzeo MC, Villagrán C, Hardacre C, Compton RG. A mechanistic study of the electro-oxidation of bromide in acetonitrile and the room temperature ionic liquid, 1-butyl-3-methylimidazolium bis (trifluoromethylsulfonyl) imide at platinum electrodes. J Electroanal Chem 2005;575:311–20.
[52] Tariq M. Electrochemistry of Br-/Br2 redox couple in acetonitrile, methanol and mix media of acetonitrile–methanol: an insight into redox behavior of bromide on platinum (Pt) and gold (Au) electrode. Z Phys Chem 2020;234:295–312.